JOURNAL OF THERMOPHYSICS AND HEAT TRANSFER
Vol. 24, No. 3, July–September 2010

Numerical Studies of Supercritical Turbulent Convective Heat Transfer of Cryogenic-Propellant Methane

Ya-Zhou Wang,* Yi-Xin Hua,* and Hua Meng†
Zhejiang University, 310027 Hangzhou, People's Republic of China

DOI: 10.2514/1.46769

In this paper, comprehensive numerical studies of the turbulent convective heat transfer of the cryogenic-propellant methane flowing inside a horizontal minitube under supercritical pressures have been conducted, based on a complete set of conservation equations and accurate evaluations of the thermophysical properties. The present numerical investigations focus on fundamental understanding of the effects of many key parameters, including the inlet pressure, wall heat flux, inlet velocity, and inlet temperature, on the supercritical heat transfer phenomena and the variations of the Nusselt number. Results indicate that drastic property variations at the pseudocritical temperature under a supercritical pressure would cause local heat transfer deterioration. Increasing the inlet methane pressure would result in improved heat transfer at supercritical pressures, particularly under a high wall heat flux, i.e., 7 MW/m^2. The conventional empirical expressions, i.e., the Gnielinski equation, cannot be used for the supercritical heat transfer predictions of the cryogenic-propellant methane at supercritical pressures. A modified heat transfer expression, which is applicable to the supercritical cryogenic methane, has been successfully established in this paper.

Nomenclature

A	=	surface area, m^2
A_n	=	coefficients in the Benedict–Webb–Rubin equation
C_p	=	constant-pressure heat capacity, J kg^{-1} K^{-1}
C_v	=	constant-volume heat capacity, J kg^{-1} K^{-1}
D	=	diameter of the tube, m
D_ω	=	cross-diffusion term in the turbulence model
e_t	=	total internal energy, J kg^{-1}
G	=	turbulent generation term
h	=	convective heat transfer coefficient, W m^{-2} K^{-1}
k	=	turbulent kinetic energy, J kg^{-1}
p	=	pressure, Pa
Pr	=	Prandtl number
Nu	=	Nusselt number
q	=	heat flux, W m^{-2}
Re	=	Reynolds number
r	=	radial coordinate, m
T	=	temperature, K
u	=	velocity, m s^{-1}
x	=	axial coordinate ($x = 0$ at the beginning of the heated section), m
Y	=	turbulent dissipation term
Γ	=	effective diffusivity, m^2 s^{-1}
γ	=	coefficient in the Benedict–Webb–Rubin equation
λ	=	thermal conductivity, W m^{-1} K^{-1}
μ	=	viscosity, kg m^{-1} s^{-1}
ρ	=	density, kg m^{-3}
τ	=	viscous stress, N m^{-2}
ω	=	specific dissipation rate, s^{-1}

Subscripts

b	=	averaged parameter
eff	=	effective value, including both laminar and turbulent parts
k	=	turbulent kinetic energy
pc	=	pseudocritical value
r	=	radial direction
w	=	wall
x	=	axial direction
ω	=	specific dissipation rate
0	=	inlet or ideal state

Received 18 August 2009; revision received 12 March 2010; accepted for publication 16 March 2010.

*Graduate Student, School of Aeronautics and Astronautics.

†Professor, School of Aeronautics and Astronautics; menghua@zju.edu.cn (Corresponding Author).

I. Introduction

METHANE is considered as a viable alternative liquid propellant for the rocket propulsion applications, and there is a renewed interest on liquid-oxygen (LOX)/methane rocket engine development. This interest stems from the unique features of the cryogenic-propellant methane compared with the other traditional liquid propellants in rocket engine applications [1,2]: i.e., its higher density, higher vaporization temperature, less-challenging storage requirements compared with the cryogenic hydrogen and its higher specific impulse, superior cooling capability, higher coking limit compared with kerosene. As a liquid propellant, methane is used as a coolant for the regenerative engine-cooling process. Since the working pressure inside the combustion chamber of a LOX/methane liquid-propellant rocket engine is generally higher than the thermodynamic critical pressure of methane, the heat transfer phenomena of methane flowing inside the engine-cooling channel before its injection would thus be under a supercritical pressure. The relevant thermodynamic properties of methane are listed in Table 1.

Under a supercritical pressure, as the temperature of methane increases during the heat transfer process, no phase change would occur, but methane would transit from a liquidlike to a gaslike state with drastic property variations within a narrow temperature range. The temperature, at which the heat capacity exhibits a maximum, is defined as the pseudocritical temperature for the corresponding supercritical pressure. The pseudocritical temperature increases with an increasing supercritical pressure. Therefore, the heat transfer phenomenon of the cryogenic-propellant methane under a supercritical pressure, which is of crucial importance for the rocket engine-cooling technology, is influenced strongly by property variations and exhibits distinct features from its subcritical counterpart.

Investigations of supercritical heat transfer phenomena have been ongoing for the past decades, but the majority of these studies are related to supercritical carbon dioxide and water, because of their

Table 1 Thermodynamic parameters of methane

Parameters	Values
Mol. wt., g/mol	16.04
Critical temperature, K	190.4
Critical pressure, bar	46
Critical volume, cm^3/mol	99.2
Critical compressibility factor	0.288
Acentric factor	0.011

practical applications in refrigeration, power plant, and nuclear energy industries. Both experimental [3–7] and numerical [8–12] studies have been conducted in detail, and the research progress has recently been summarized [13,14]. A number of research work has also been conducted concerning the supercritical heat transfer of hydrocarbon fuels [15–17], mainly with kerosene for its crucial importance in engine-cooling technology in the rocket and airbreathing hypersonic propulsion systems. Very few studies [18] of supercritical heat transfer with the cryogenic-propellant methane could be found in the open literature.

The existing studies of supercritical heat transfer clearly indicated that the related processes were very complex and affected significantly by the strong property variations, especially in the vicinity of the pseudocritical temperature under a supercritical pressure. In addition, the supercritical heat transfer processes would behave differently under different heat fluxes. For example, with the supercritical carbon dioxide and water, heat transfer would be enhanced in the vicinity of the pseudocritical temperature under a low heat flux, but it could be deteriorated under a high heat flux. Since the supercritical heat transfer processes are closely related to property variation and heat flux and the property variations of the cryogenic-propellant methane significantly differ from carbon dioxide and water (moreover, the heat flux in a liquid-propellant rocket engine is much higher than those in the other conventional industrial applications), the turbulent heat transfer phenomena of the cryogenic-propellant methane under supercritical pressures could differ dramatically from those of carbon dioxide or water. Therefore, the applicability of the existing research results concerning the supercritical heat transfer of carbon dioxide and water to the supercritical cryogenic-propellant methane has to be determined. Because of its crucial importance for the rocket engine-cooling technology, the supercritical heat transfer of methane demands thorough investigations.

In this paper, comprehensive numerical studies of the turbulent heat transfer of the cryogenic-propellant methane flowing inside a horizontal minitube under supercritical pressures have been conducted, focusing on fundamental understanding of the effects of the property variations on the heat transfer processes. The present numerical investigations are based on a complete set of conservation equations of mass, momentum, and energy, and incorporate accurate calculations of the thermodynamic and transport properties of methane at different temperatures and pressures. The effects of many key parameters, including the inlet pressure, wall heat flux, inlet velocity, and inlet temperature, on the supercritical heat transfer phenomena of the cryogenic-propellant methane have been studied in detail.

II. Theoretical Formulation

The present numerical studies of the turbulent heat transfer of the cryogenic-propellant methane under supercritical pressures focus on fundamental understanding. A complete set of conservation equations of mass, momentum, and energy are numerically solved within an axisymmetric plane. Since the tube diameter is very small, i.e., 2 mm, and the forced-flow velocity is sufficiently high, i.e., ≥ 10 m/s, the buoyancy effect is small and is temporarily neglected in the present numerical studies, focusing solely on the forced-flow heat transfer phenomena. The conservation equations are provided in the following forms.

Mass conservation:

$$\frac{\partial}{\partial x}(\rho u_x) + \frac{1}{r}\frac{\partial}{\partial r}(\rho r u_r) = 0 \tag{1}$$

Momentum conservation:

$$\frac{\partial}{\partial x}(\rho u_x u_x) + \frac{1}{r}\frac{\partial}{\partial r}(r\rho u_x u_r) = -\frac{\partial p}{\partial x} + \frac{\partial \tau_{xx}}{\partial x} + \frac{1}{r}\frac{\partial}{\partial r}(r\tau_{xr}) \tag{2}$$

$$\frac{\partial}{\partial x}(\rho u_r u_x) + \frac{1}{r}\frac{\partial}{\partial r}(r\rho u_r u_r) = -\frac{\partial p}{\partial r} + \frac{\partial \tau_{rx}}{\partial x} + \frac{1}{r}\frac{\partial}{\partial r}(r\tau_{rr}) \tag{3}$$

Energy conservation:

$$\frac{\partial}{\partial x}(\rho u_x e_t) + \frac{1}{r}\frac{\partial}{\partial r}(r\rho u_r e_t) = \frac{\partial}{\partial x}\left[\lambda_{\text{eff}}\frac{\partial T}{\partial x}\right] + \frac{1}{r}\frac{\partial}{\partial r}\left[r\lambda_{\text{eff}}\frac{\partial T}{\partial r}\right] \tag{4}$$

In Eqs. (2) and (3), the standard viscous terms are employed without any modification. The supercritical pressure effect on these terms is through property variations. The viscous terms are defined as

$$\tau_{xx} = \mu_{\text{eff}}\left[2\frac{\partial u_x}{\partial x} - \frac{2}{3}(\nabla \cdot \mathbf{u})\right] \tag{5a}$$

$$\tau_{rr} = \mu_{\text{eff}}\left[2\frac{\partial u_r}{\partial r} - \frac{2}{3}(\nabla \cdot \mathbf{u})\right] \tag{5b}$$

$$\tau_{xr} = \tau_{rx} = \mu_{\text{eff}}\left[\frac{\partial u_x}{\partial r} + \frac{\partial u_r}{\partial x}\right] \tag{5c}$$

$$\nabla \cdot (\mathbf{u}) = \frac{\partial u_x}{\partial x} + \frac{1}{r}\frac{\partial}{\partial r}(r u_r) \tag{5d}$$

In the present numerical studies, since the heat flux enforced at the tube wall is higher than 1 MW/m^2, and the thermophysical properties vary significantly in the near-wall region, we chose the shear stress transport k-ω turbulent model [19,20] for the internal turbulent flow and heat transfer calculations. The key advantage of this turbulent model is its direct validity in the near-wall region, including the viscous sublayer, thus avoiding the implementation of an uncertain wall function. The turbulent equations are presented as follows:

$$\frac{\partial}{\partial x}(\rho k u_x) + \frac{1}{r}\frac{\partial}{\partial r}(r\rho k u_r) = \frac{\partial}{\partial x}\left[\Gamma_k\frac{\partial k}{\partial x}\right] + \frac{1}{r}\frac{\partial}{\partial r}\left[r\Gamma_k\frac{\partial k}{\partial r}\right] + G_k - Y_k \tag{6}$$

$$\frac{\partial}{\partial x}(\rho \omega u_x) + \frac{1}{r}\frac{\partial}{\partial r}(r\rho \omega u_r) = \frac{\partial}{\partial x}\left[\Gamma_\omega\frac{\partial \omega}{\partial x}\right] + \frac{1}{r}\frac{\partial}{\partial r}\left[r\Gamma_\omega\frac{\partial \omega}{\partial r}\right] + G_\omega - Y_\omega + D_\omega \tag{7}$$

All the standard terms in the SST k-ω turbulent model are implemented in the present numerical studies without any modification. The supercritical pressure effect on these two equations is through property variations. Details concerning this turbulent model and its various terms can be found in [19,20] and are thus not repeated in this paper.

A. Boundary Conditions

The physical problem of concern involves the cryogenic-propellant methane flowing inside a horizontal minitube with constant wall heat flux enforced in the middle section of 300 mm long, as shown in Fig. 1. The beginning unheated section with a

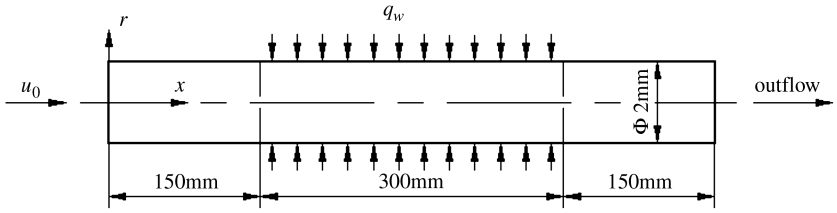

Fig. 1 Schematic configuration.

length of 150 mm is used to obtain a fully developed flowfield before the heat transfer process, and the ending unheated section of 150 mm long is included to avoid the effects of outflow boundary condition on the numerical results. The boundary conditions are defined as follows.

Inlet boundary conditions:

$$u_x = u_0, \quad u_r = 0, \quad T = T_0, \quad p = p_0, \quad k = k_0, \quad \omega = \omega_0 \tag{8}$$

Outflow boundary conditions:

$$\frac{\partial u_x}{\partial x} = \frac{\partial u_r}{\partial x} = \frac{\partial T}{\partial x} = \frac{\partial p}{\partial x} = \frac{\partial k}{\partial x} = \frac{\partial \omega}{\partial x} = 0 \tag{9}$$

Axisymmetric boundary conditions:

$$\frac{\partial u_x}{\partial r} = \frac{\partial T}{\partial r} = \frac{\partial p}{\partial r} = \frac{\partial k}{\partial r} = \frac{\partial \omega}{\partial r} = 0 \qquad u_r = 0 \tag{10}$$

Wall boundary conditions for the heated section:

$$u_x = u_r = 0, \qquad q = q_w, \qquad \frac{\partial p}{\partial r} = \frac{\partial k}{\partial r} = 0 \tag{11}$$

Wall boundary conditions for the two unheated sections:

$$u_x = u_r = 0, \qquad q = 0, \qquad \frac{\partial p}{\partial r} = \frac{\partial k}{\partial r} = 0 \tag{12}$$

In the wall boundary definitions, the specific dissipation rate ω in the wall-adjacent cell is directly computed using the law of the wall [19,20], and thus no boundary value is needed.

B. Property Evaluations

A key for obtaining accurate numerical results in supercritical heat transfer lies in accurate and robust property calculations, since property variations significantly influence the heat transfer processes. To calculate the thermodynamic properties of methane, including its heat capacity and internal energy, the fundamental thermodynamic theories could be applied to derive the relevant expressions [21,22]. For example, the following expression for the heat capacity can be derived [21]:

$$C_p(T,\rho) = C_{v0}(T) - \int_{\rho_0}^{\rho}\left[\frac{T}{\rho^2}\left(\frac{\partial^2 p}{\partial T^2}\right)_\rho\right]_T \mathrm{d}\rho + \frac{T}{\rho^2}\left(\frac{\partial p}{\partial T}\right)_\rho^2 \Big/ \left(\frac{\partial p}{\partial \rho}\right)_T \tag{13}$$

where all the variables are defined in the nomenclature. A Soave–Redlich–Kwong (SRK) equation of state is combined with Eq. (13) to obtain the numerical values of the heat capacity, as the SRK equation of state is relatively simple and accurate [21,22].

The extended corresponding-state method [23,24] could be used for evaluating the transport properties of a supercritical fluid, including its viscosity and thermal conductivity at different temperatures and pressures. Since methane is generally used as the reference material in this method, accurate empirical expressions exist for directly evaluating these properties of methane [23,24]. However, in order to use these expressions, a modified Benedict–Webb–Rubin (BWR) equation of state is required to obtain the density of methane at various conditions. The BWR equation of state can be expressed in the following form:

$$p = \sum_{n=1}^{9} A_n(T)\rho^n + \sum_{n=10}^{15} A_n(T)\rho^{2n-17}e^{-\gamma\rho^2} \tag{14}$$

The empirical parameters in this equation can be found in [23]. This complex equation of state is needed to obtain the methane density very accurately, because the precision of the density calculation dramatically affects the transport properties.

The property-evaluation methods discussed in this section have been used to obtain the density, heat capacity, viscosity, and thermal conductivity of the cryogenic methane, as shown in Fig. 2. The calculated results have been compared with the National Institute of Standards and Technology data,[‡] showing excellent agreement. This further verifies the accuracy of the present property-evaluation methods.

III. Results and Discussion

Before numerical calculations, a grid-independence study has been conducted to ensure numerical accuracy. As stated in the previous section, since the SST k-ω turbulent model has been employed in the present numerical studies, the first grid close to the wall has to be put inside the viscous sublayer. Our grid-independence study indicates that a grid system of 70×8000 meshes in the radial and axial directions is sufficient for the present numerical calculations. The meshes in the axial direction are clustered toward the wall with a stretch ratio of 1.1, which results in the first grid close to the wall satisfying $y^+ \leq 1$, well within the viscous sublayer.

Model validation has also been conducted before the detailed numerical calculations. Since consistent and reliable experimental data exist for the supercritical heat transfer of carbon dioxide flowing inside a minitube, we based our model validation on the experimental results of supercritical carbon dioxide [11]. The numerical and experimental results are compared in Fig. 3. The differences between the numerical and experimental data are generally within 10%, further verifying the validity and accuracy of the present numerical treatment.

After model validation and numerical verification, numerical studies of turbulent convective heat transfer of the cryogenic-propellant methane flowing inside a minitube under supercritical pressures have been conducted, focusing on the effects of many key parameters on the heat transfer processes. Those parameters include the pressure, inlet velocity, wall heat flux, and inlet temperature.

A. Effects of Pressure

The effects of the supercritical pressure on the heat transfer processes have been first studied with a low heat flux enforced at the heated section of the tube wall, as shown in Fig. 1. The constant wall heat flux in this case is 3 $\mathrm{MW/m^2}$, which is a relatively low value for a booster-stage liquid-propellant rocket engine. The four different pressures, which are defined at the tube inlet, are 6, 8, 10, and 12 MPa, respectively. These pressures are all above the critical pressure of methane at 46 bar, as listed in Table 1. In this case, the inlet temperature of methane is 120 K and the inlet velocity is 25 m/s. The corresponding Reynolds and Prandtl numbers are 1.9×10^5 and 1.82, respectively.

[‡]Data available online at http://webbook.nist.gov/chemistry/fluid [retrieved 13 April 2010].

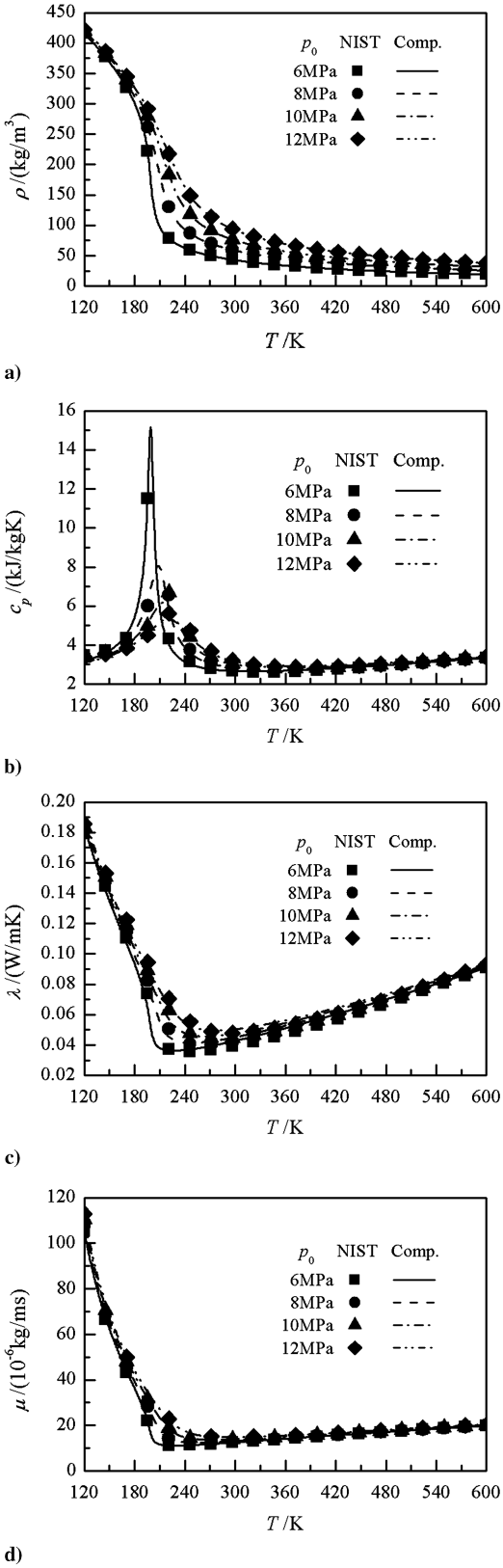

Fig. 2 Calculated thermophysical properties of methane: a) density, b) heat capacity, c) thermal conductivity, and d) viscosity.

The variations of the wall temperature and the averaged methane temperature at the four different pressures are presented in Fig. 4. The averaged fluid temperature is defined as

$$T_b = \int_A \rho u_x C_p T \, \mathrm{d}A \Big/ \int_A \rho u_x C_p \, \mathrm{d}A \tag{15}$$

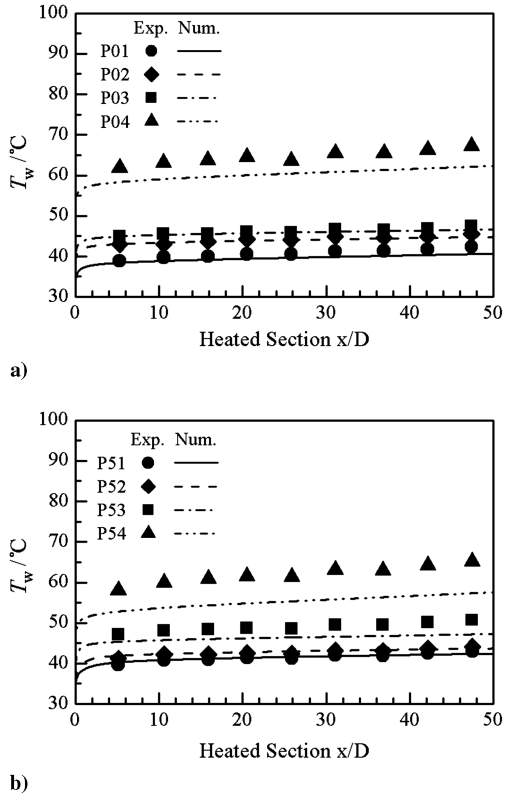

Fig. 3 Model validation against experimental data in [11]: a) P01 is 9.59 MPa, P02 is 9.54 MPa, P03 is 9.5 MPa, P04 is 9.43 MPa and b) P51 is 8.46 MPa, P52 is 8.46 MPa, P53 is 8.47 MPa, and P54 is 8.48 MPa.

As shown in Fig. 4b, the averaged methane temperature increases slightly with the increasing pressure, due mainly to the density and heat capacity variations under different supercritical pressures, but the difference is very small. The typical temperature distribution of methane inside the minitube at 8 MPa is further illustrated in Fig. 5. This figure clearly illuminates that the methane temperature increases drastically near the tube wall, at which the constant wall heat flux is enforced.

A very interesting phenomenon could be observed in Fig. 4a concerning the wall temperature variation at a pressure of 6 MPa; it increases sharply around $x/D = 45$ ($x/D = 0$ refers to the start of the heated section), corresponding to heat transfer deterioration. As can be seen in Fig. 4a, under 6 MPa and at $x/D = 45$, the wall temperature reaches around 190 K, the pseudocritical temperature of methane at the corresponding supercritical pressure. Once the wall temperature reaches the pseudocritical temperature, the thermophysical properties of methane, including its heat capacity and thermal conductivity, decreases abruptly at the tube wall, as shown in Fig. 6. As the thermal conductivity and heat capacity of methane at the tube wall decreases, its capabilities to transfer and absorb energy decrease accordingly, resulting in the sharp increase of the wall temperature. Therefore, the sharp wall temperature variation at 6 MPa is closely related to the thermophysical property variations in the pseudocritical temperature region at the tube wall. The abrupt property variations at 6 MPa at $x/D = 45$ also render slight flowfield and wall temperature oscillations.

Heat transfer deterioration also occurs at 8 MPa around $x/D = 70$, as shown in Fig. 4a, but in this case, the sudden temperature increase is much weaker, consistent with the weak decrease of the thermophysical properties at 8 MPa at the tube wall, as also illustrated in Fig. 6.

To quantitatively comprehend the effects of the supercritical pressure on the heat transfer processes and, in the mean time, explore the applicability of the conventional heat transfer formula at supercritical pressures, we have calculated the corresponding Nusselt number under the four different supercritical pressures and compared results with those obtained from the empirical formula,

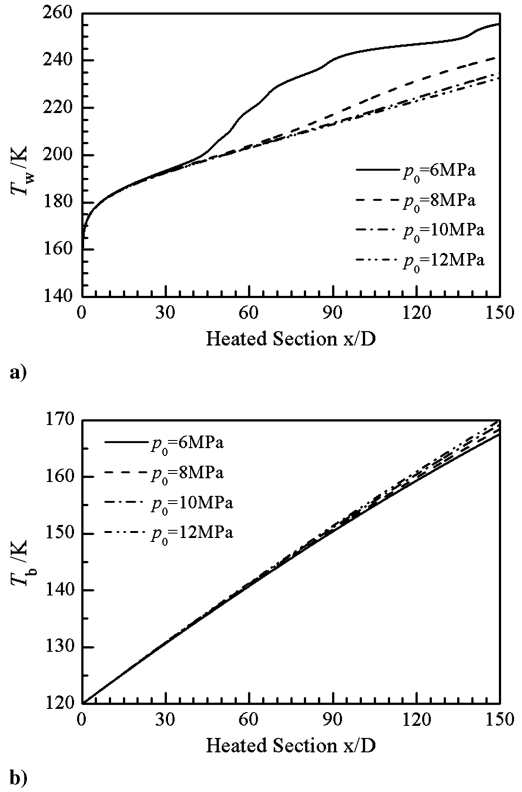

Fig. 4 Temperature variations with a wall heat flux of 3 MW/m^2 under different supercritical pressures ($T_0 = 120$ K and $u_0 = 25$ m/s): a) wall temperature and b) averaged methane temperature.

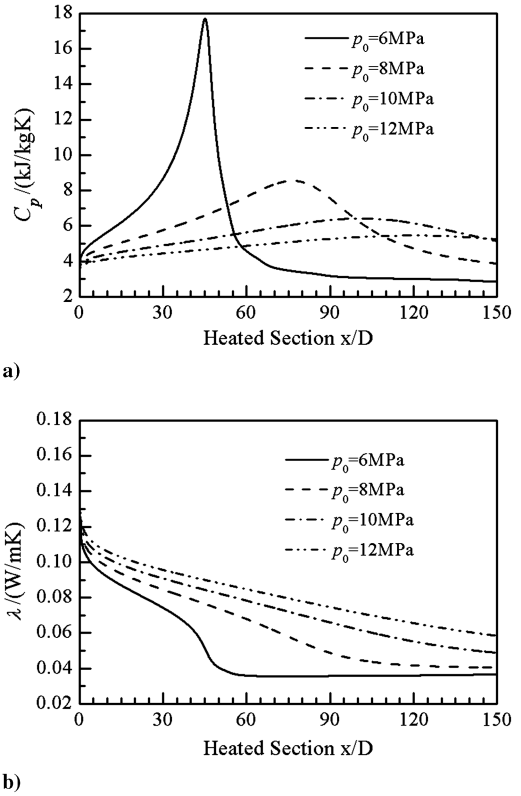

Fig. 6 Thermophysical property variations along the tube wall ($q_w = 3$ MW/m^2, $T_0 = 120$ K, and $u_0 = 25$ m/s): a) heat capacity and b) thermal conductivity.

including the conventional Sieder–Tate and Gnielinski heat transfer expressions, and both could only accommodate mild property variations [25]. The Nusselt number is defined as

$$Nu = \frac{hD}{\lambda_b} \tag{16}$$

Since the Gnielinski expression provides better comparisons with the present numerical results, only this expression will be used in the following discussion. As shown in Fig. 7a, the calculated Nusselt number sharply decreases within $x/D = 10$, because of the fluid is suddenly heated. This thermal entrance effect would be neglected in the following discussion. In Fig. 7a, as the pressure increases, the Nusselt number from the present numerical calculations increases, while the difference between the empirical formula and the numerical calculations decreases. The results from the Gnielinski expression become close to the numerical results as the pressure increases, and at a pressure above 10 MPa, it could be used for the supercritical heat transfer calculations with a reasonable accuracy. At a pressure of 6 MPa, the Nusselt number from the numerical results shows a sharp decrease at $x/D = 45$, corresponding to the sharp increase of the wall temperature in the same location. This sharp variation cannot be predicted using the conventional empirical expressions, i.e., the Gnielinski formula.

Given the very limited applicability of the conventional heat transfer formula, attempts have been made to search for a proper expression for predicting the supercritical heat transfer coefficient of the cryogenic methane. It is found that a heat transfer expression proposed by Jackson and Hall [26] for the supercritical carbon dioxide and water can be slightly modified for this purpose. In another study by our group [27], a slightly different version of this expression has also been proved to be valid for predicting the supercritical heat transfer coefficient of a typical liquid propellant, *n*-heptane. The modified heat transfer expression is established in the following form:

$$Nu_D = 0.0156 Re_b^{0.82} Pr_b^{0.5} \left(\frac{\rho_w}{\rho_b}\right)^{0.3} \left(\frac{\bar{C}_p}{C_{pb}}\right)^n \tag{17}$$

where the parameters $\bar{C}_p$ and n are defined as

$$\bar{C}_p = (H_w - H_b)/(T_w - T_b) \tag{18}$$

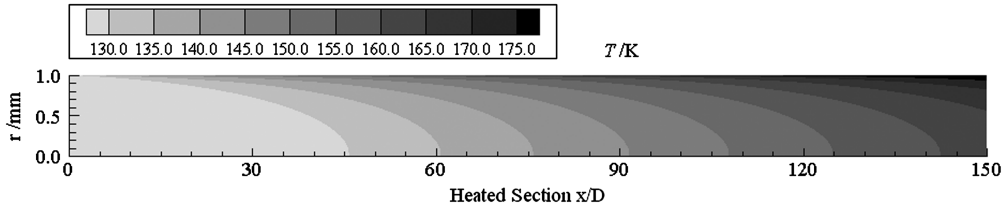

Fig. 5 Temperature distribution with a wall heat flux of 3 MW/m^2 and under a supercritical pressure of 8 MPa ($T_0 = 120$ K and $u_0 = 25$ m/s).

$$n = \begin{cases} 0.4 & \text{for } T_b < T_w \le T_{\text{pc}} \quad \text{or} \quad 1.2T_{\text{pc}} \le T_b < T_{\text{w}} \\ 0.4 + 0.2\left(\frac{T_w}{T_{\text{pc}}} - 1\right) & \text{for } T_b \le T_{\text{pc}} < T_w \\ 0.4 + 0.2\left(\frac{T_w}{T_{\text{pc}}} - 1\right)\left[1 - 5\left(\frac{T_b}{T_{\text{pc}}} - 1\right)\right] & \text{for } T_{\text{pc}} < T_b \le 1.2T_{\text{pc}} \quad \text{and} \quad T_b < T_w \end{cases} \tag{19}$$

This expression is chosen to obtain an optimum fit for all the cases studied in the present paper, including those presented in the next sections.

As illustrated in Fig. 7b, the modified heat transfer expression in Eq. (17) performs much better than the Gnielinski formula under the four different pressures. The two sets of results both increase as the pressure increases. More important, this modified expression can correctly predict the sudden decrease of the Nusselt number under 6 and 8 MPa when the fluid temperature at the wall reaches the corresponding pseudocritical temperature of methane. The relative errors between the two sets of results are within 20%, very good for an empirical heat transfer expression. The superiority of this modified expression is attributable to its accommodation of strong property variations in the pseudocritical temperature region, while the conventional heat transfer formula, i.e., the Gnielinski formula, can only account for mild property variations at a very high pressure, i.e., 10 MPa, under which the effect of the pseudocritical temperature on property variations is alleviated.

The effects of the supercritical pressure on the heat transfer processes have also been studied with a high wall heat flux of 7 MW/m^2 enforced at the heated section of the cooling tube, while all the other relevant parameters remain the same. The variations of the wall temperature and the averaged methane temperature are presented in Fig. 8. Under the four different pressures, the wall temperature decreases with the increasing pressure, as shown in Fig. 8a. This trend indicates that the supercritical heat transfer process under a high wall heat flux could be enhanced as the pressure increases.

The averaged methane temperature under the four different pressures shows little difference until $x/D = 90$. After that, the difference of the averaged temperature increases with the increasing pressure, and at the end of the heated section, it could reach more than 20 K, as shown in Fig. 8b.

At the two supercritical pressures of 6 and 8 MPa, the wall temperature shows sharp increase during the heat transfer process, as shown in Fig. 8a. Since the wall temperatures for both cases are well above the corresponding pseudocritical temperatures at the two supercritical pressures, the physics underlying this intriguing phenomenon is apparently different from the low-heat-flux cases. In fact, the sharp wall temperature increase in Fig. 8a results from drastic property variations in a region near the wall in these high-heat-flux cases, compared with the significant property variations at the wall in those low-heat-flux cases. As shown in Fig. 9, at a supercritical pressure of 8 MPa, the pseudocritical temperature is reached from around $x/D = 95$ in a relatively large region near the wall in a range of r/r_0 from 0.967 to 0.859. Therefore, abrupt property variations occur in this near-wall region and lead to the sharp wall temperature increase. The distribution of the heat capacity at 8 MPa is also illuminated in Fig. 9.

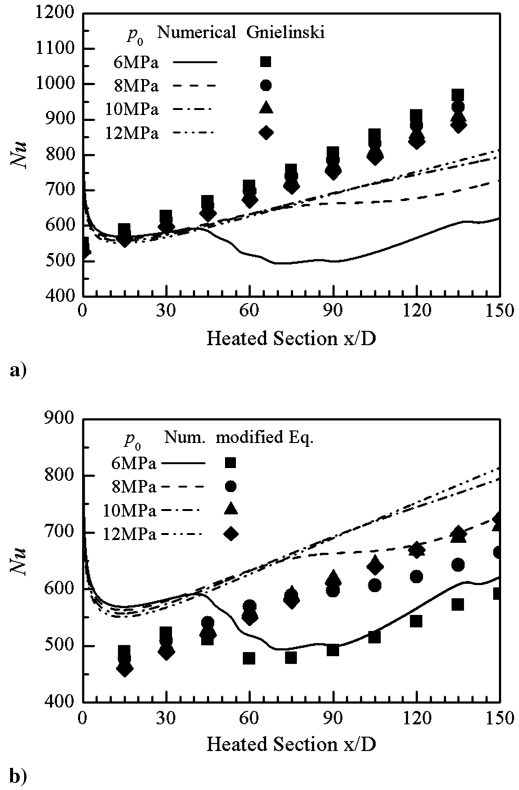

Fig. 7 Comparisons of the Nusselt number from the present numerical calculations and the empirical expressions under different pressures ($q_w = 3$ MW/m^2, $T_0 = 120$ K, and $u_0 = 25$ m/s): a) against the Gnielinski equation and b) against the modified equation.

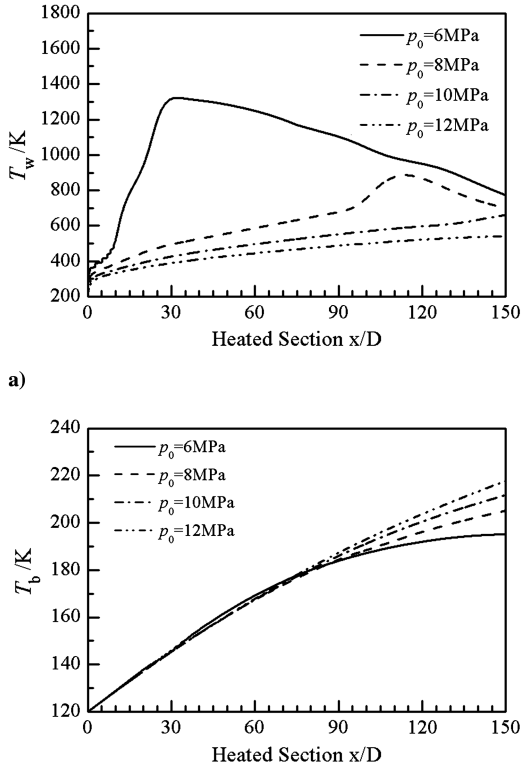

Fig. 8 Temperature variations with a wall heat flux of 7 MW/m^2 under different supercritical pressures ($T_0 = 120$ K and $u_0 = 25$ m/s): a) wall temperature and b) averaged methane temperature.

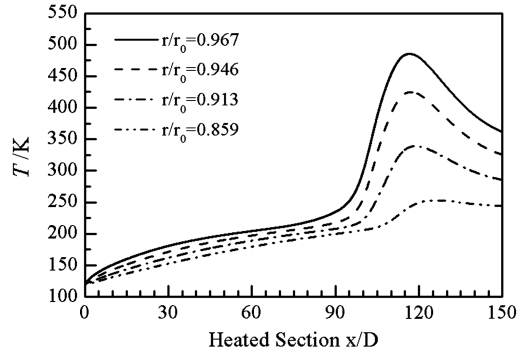

a)

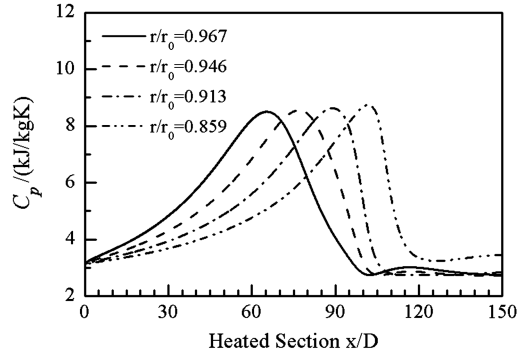

b)

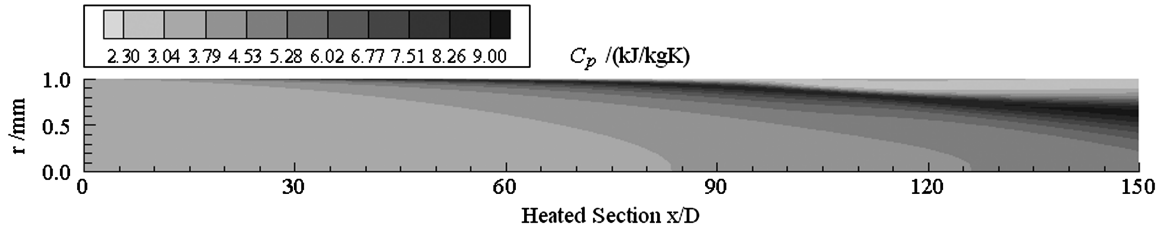

c)

Fig. 9 Temperature and thermophysical properties in the near-wall region ($q_w = 7$ MW/m^2, $T_0 = 120$ K, $u_0 = 25$ m/s, and $p_0 = 8$ Mpa): a) temperature variation, b) heat capacity variation, and c) heat capacity contour.

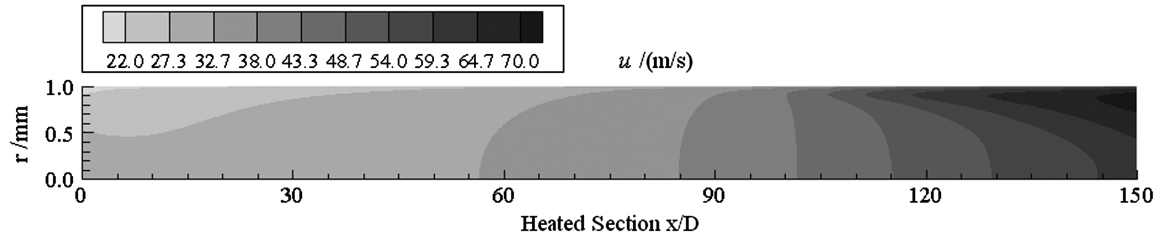

a)

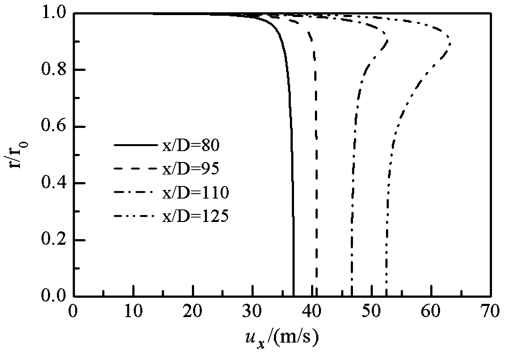

b)

Fig. 10 Velocity variations at 8 MPa ($q_w = 7$ MW/m^2, $T_0 = 120$ K, and $u_0 = 25$ m/s): a) velocity distribution in the flowfield and b) axial velocity variations in different downstream locations.

As temperature increases, density would decreases accordingly, as illustrated in Fig. 2. To maintain a constant mass flux, the flow velocity must increase along the axial direction. As depicted in Fig. 10, starting from $x/D = 100$, the abrupt density decrease in the near-wall region results in drastic velocity increase. The increased flow velocity enhances the convective heat transfer process, and thus starting from $x/D = 120$, this favorable process of heat transfer enhancement overweighs the adverse effect of heat transfer deterioration resulting from the density and heat capacity decrease, leading to the gradual decrease of the wall temperature from that location.

The Nusselt number obtained from the Gnielinski equation and the present numerical calculations under the four different supercritical pressures is compared in Fig. 11a. In these high-wall-heat-flux cases, the difference between the two sets of results becomes very large. For the empirical results, the Nusselt number decreases as the pressure increases, but the numerical results varies in an exactly opposite trend. As a result, the difference between the two sets of results becomes smaller as pressure increases, but the empirical expression still remains invalid even at a very high pressure of 12 MPa under this high wall heat flux of 7 MW/m^2.

Comparisons between the numerical results and those from the modified heat transfer expression in Eq. (17) are further illustrated in Fig. 11b. The two sets of results both increase as the pressure increases, clearly indicating heat transfer enhancement with pressure. Under this high wall heat flux, the modified heat transfer expression shows very good accuracy under 10 and 12 MPa, with the relative error within 25%. At a pressure of 8 MPa, the modified expression also performs well, capable of predicting the sharp heat transfer deterioration around the pseudocritical temperature region; the relative error is within 25% for the majority of the heated section except at the transitional region in which the heat transfer deterioration occurs. In the transitional region, the maximum relative error could reach 40% at 8 MPa. As the supercritical pressure decreases to 6 MPa, since the thermophysical properties experience much stronger variations under a high wall heat flux of 7 MW/m^2, the modified heat transfer expression fails to predict the correct trend. Further investigation is still needed for this particular case.

B. Effects of Inlet Velocity

The effects of the inlet velocity on the supercritical convective heat transfer processes are investigated in this section. The inlet velocity varies from 10 to 30 m/s, covering the entire practical range in rocket propulsion applications, the inlet supercritical pressure in all these cases is fixed at 8 MPa, the inlet methane temperature at 120 K, while the constant wall heat flux at 3 MW/m^2. The variations of the wall temperature and the averaged methane temperature are depicted in Fig. 12. Results indicate that the averaged methane temperature and the wall temperature both decrease as the inlet velocity increases, a phenomenon attributable to the enhanced convective heat transfer at a high inlet velocity.

As shown in Fig. 12a, at a low inlet velocity of 10 m/s, the wall temperature sharply increases from $x/D = 100$, reaches a highest value at around 700 K, and then decreases gradually afterward. The underlying physics for this heat transfer process is the same as that under a high wall heat flux of 7 MW/m^2 discussed in the early section; starting from $x/D = 100$, the local temperature in the near-wall region reaches the pseudocritical temperature at 8 MPa and consequently results in the abrupt density and heat capacity decrease, as illustrated in Fig. 13. The decreased density and heat capacity lead to heat transfer deterioration. As density decreases, the flow velocity near the wall increases, as shown clearly in Fig. 13c. The increased flow velocity then enhances the heat transfer process and renders the wall temperature to decrease subsequently.

The conventional heat transfer expressions, i.e., the Gnielinski equation, perform poorly, except at a high inlet velocity of 30 m/s, and thus could not be applied directly for supercritical heat transfer predictions in these cases. As shown in Fig. 14, the modified heat transfer expression, on the other hand, exhibits very good performance; it can not only predict the increasing trend of the Nusselt number as the inlet velocity increases, but also correctly predict the

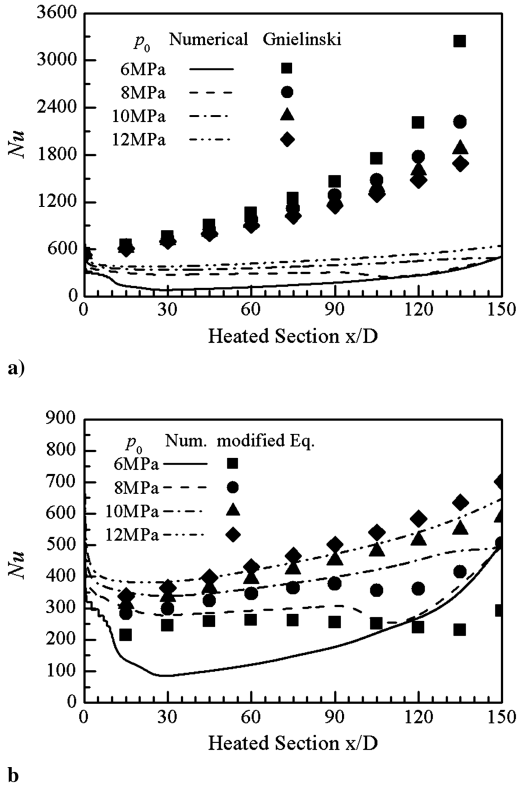

Fig. 11 Comparisons of the Nusselt number from the present numerical calculations and the empirical expressions under different pressures ($q_w = 7$ MW/m^2, $T_0 = 120$ K, and $u_0 = 25$ m/s): a) against the Gnielinski equation and b) against the modified equation.

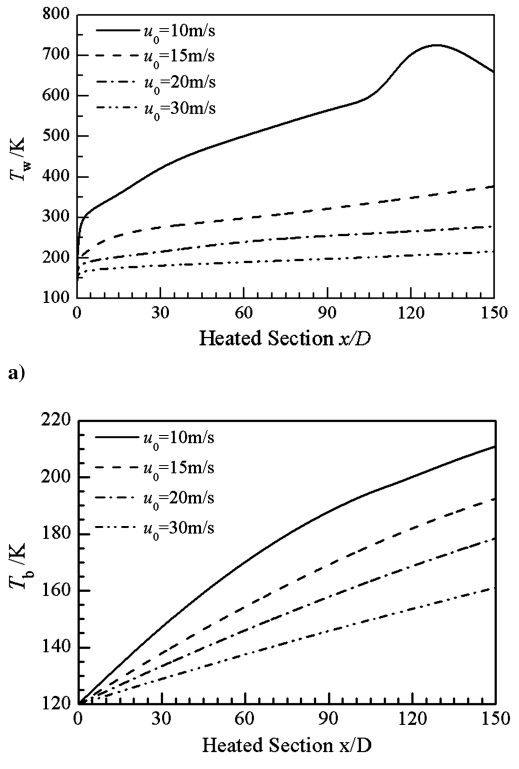

Fig. 12 Temperature variations at different inlet velocities ($q_w =$ 3 MW/m^2, $T_0 = 120$ K, and $p_0 = 8$ MPa): a) wall temperature and b) averaged methane temperature.

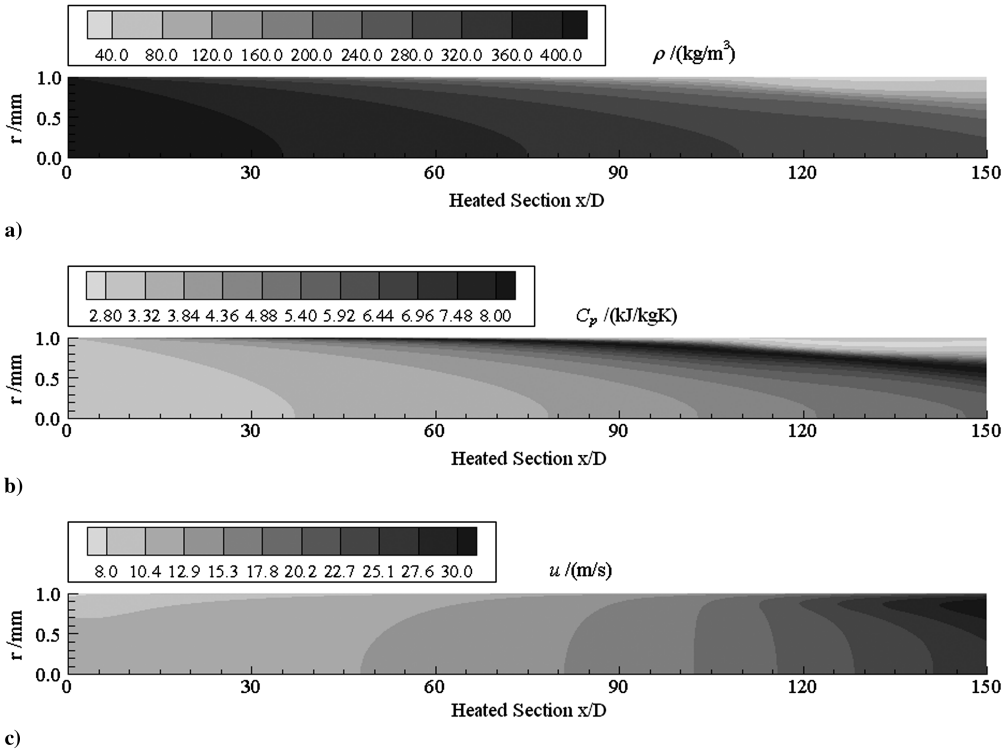

Fig. 13 Thermophysical property and velocity distributions with an inlet velocity at 10 m/s ($q_w = 3$ MW/m^2, $T_0 = 120$ K, and $p_0 = 8$ MPa): a) density, b) heat capacity, and c) velocity.

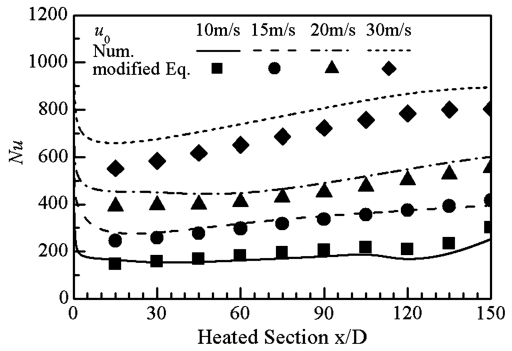

Fig. 14 Comparisons of the Nusselt number from the present numerical calculations and the modified equation at different inlet velocities ($q_w = 3$ MW/m^2, $T_0 = 120$ K, and $p_0 = 8$ MPa).

transitional location at which the sudden decrease of the Nusselt number occurs at a inlet velocity of 10 m/s. The relative errors between the numerical and the predicted results are well within 25% for all the cases studied.

C. Effects of Heat Flux

The effects of the wall heat flux on the supercritical heat transfer processes are thoroughly studied, as well. The wall heat flux ranges from 1 to 7 MW/m^2, the supercritical pressure is fixed at 8 MPa, the methane inlet temperature at 120 K, the inlet velocity at 25 m/s. Figure 15 presents the variations of the wall and the averaged methane temperature under the four different wall heat fluxes. As the wall heat flux increases, both the wall and the averaged methane temperature increase accordingly, as expected. At a high heat flux of 7 MW/m^2, the wall temperature shows a sharp increase starting from $x/D = 95$: it reaches a highest value at 900 K and then decreases gradually afterward. The underlying physics for this case has been discussed in the early section and is thus not repeated here.

Based on the present numerical studies, it is concluded that the conventional heat transfer expressions, i.e., the Gnielinski equation, cannot be used for supercritical heat transfer of the cryogenic methane owing to strong property variations. Figure 16 shows the variations of the Nusselt number from both the modified equation (17) and the present numerical calculations under the four different wall heat fluxes. The two sets of results agree very well, with

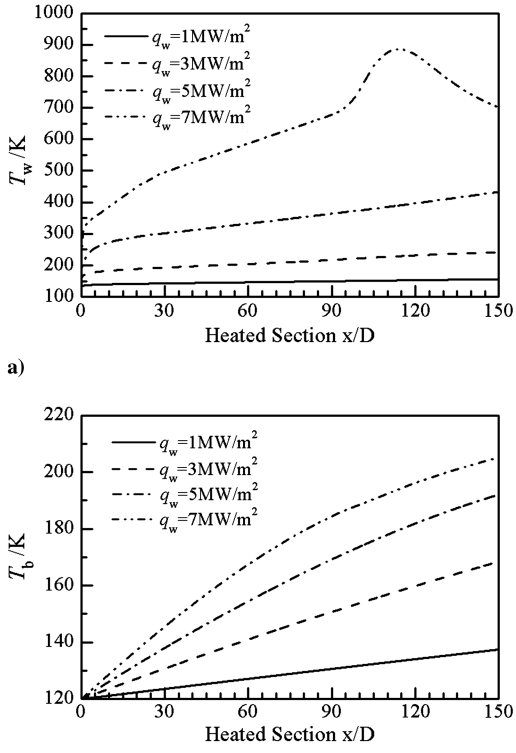

Fig. 15 Temperature variations with different wall heat fluxes ($T_0 = 120$ K, $u_0 = 25$ m/s, and $p_0 = 8$ MPa): a) wall temperature and b) averaged methane temperature.

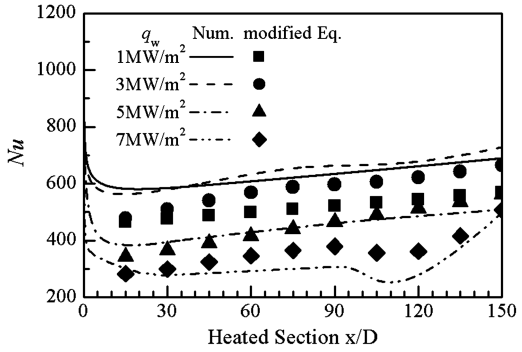

Fig. 16 Comparisons of the Nusselt number from the present numerical calculations and the modified equation under different wall heat fluxes ($T_0 = 120$ K, $u_0 = 25$ m/s, and $p_0 = 8$ MPa).

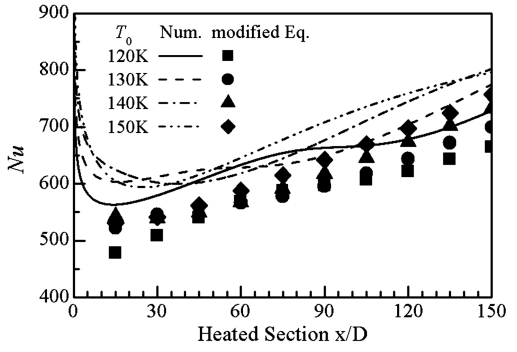

Fig. 18 Comparisons of the Nusselt number from the present numerical calculations and the modified equation at different inlet temperatures ($q_w = 3$ MW/m^2, $u_0 = 25$ m/s, and $p_0 = 8$ MPa).

relative errors within 25%. Moreover, numerical results reveal that the Nusselt number increases slightly as the wall heat flux varies from 1 to 3 MW/m^2, but it starts to decrease as the wall heat flux further increases from 3 to 7 MW/m^2. This variation trend is exactly predicted by the modified heat transfer expression, clearly proving its applicability and robustness at different wall heat fluxes.

D. Effects of Inlet Temperature

The effects of the inlet methane temperature on the supercritical heat transfer phenomena are finally discussed in this section. The inlet methane temperature ranges from 120 to 150 K, maintaining a value well below its pseudocritical temperature, the inlet pressure is fixed at 8 MPa, the inlet velocity at 25 m/s, and the constant wall heat flux at 3 MW/m^2. Figure 17 illustrates the variations of the wall and the averaged methane temperature at the four different inlet temperatures. Both types of temperature increase with the increasing inlet methane temperature.

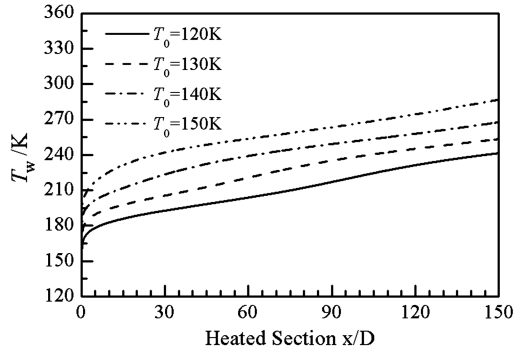

a)

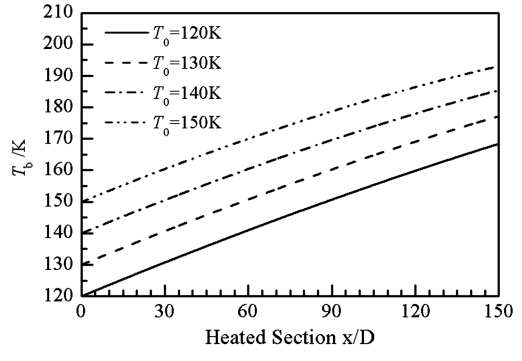

b)

Fig. 17 Temperature variations at different inlet temperatures ($q_w = 3$ MW/m^2, $u_0 = 25$ m/s, and $p_0 = 8$ MPa): a) wall temperature and b) averaged methane temperature.

Figure 18 shows the variations of the Nusselt number from both the modified equation (17) and the present numerical calculations. Both sets of results indicate that the Nusselt number slightly increases as the inlet methane temperature increases, but the variation is very limited. Although the data obtained from the modified expression fall below the numerical results, the relative errors between them are well within 20%, very good for an empirical heat transfer expression.

IV. Conclusions

In this paper, comprehensive numerical studies of the turbulent convective heat transfer of the cryogenic-propellant methane flowing inside a horizontal minitube under supercritical pressures have been conducted, intended for the engine regenerative cooling technology in rocket propulsion applications. The numerical investigations are based on a complete set of conservation equations of mass, momentum, and energy, and incorporate accurate evaluations of the thermodynamic and transport properties of methane at different temperatures and pressures. The present numerical studies focus on fundamental understanding of the effects of many key parameters, including the inlet pressure, wall heat flux, inlet velocity, and inlet temperature, on the supercritical heat transfer phenomena. The Nusselt number obtained from the present numerical calculations has been compared with that from the conventional empirical formula, i.e., the Gnielinski equation, showing the inapplicability of these conventional heat transfer formula for the supercritical cryogenic methane. A modified supercritical heat transfer expression has been successfully established in this paper, based on the heat transfer equation proposed by Jackson and Hall for the supercritical carbon dioxide and water. The following conclusions could be reached:

1) Close to the pseudocritical temperature under a supercritical pressure, drastic property variations would lead to local heat transfer deterioration and sharp increase of the wall temperature.

2) Under supercritical pressures, increasing the inlet methane pressure would result in improved heat transfer, particularly with a high heat flux enforced at the tube wall, i.e., 7 MW/m^2.

3) The conventional empirical formula, i.e., the Gnielinski equation, generally cannot be used for the supercritical heat transfer predictions of methane, since they cannot accommodate strong property variations.

4) A modified supercritical heat transfer expression has been established in this paper for the supercritical heat transfer predictions of the cryogenic-propellant methane, showing very good accuracy except when the pressure is below 8 MPa and the wall heat flux above 7 MW/m^2.

Acknowledgment

This research work is financially supported by the National Natural Science Foundation of China (no. 10972197).

References

[1] Burkhardt, H., Sippel, M., Herbertz, A., and Klevanski, J., "Kerosene vs Methane: A Propellant Tradeoff for Reusable Liquid Booster Stages," *Journal of Spacecraft and Rockets*, Vol. 41, No. 5, 2004, pp. 762–769. doi:10.2514/1.2672

[2] Marshall, W. M., Pal, S., Woodward, R. D., and Santoro, R. J., "Combustion Instability Studies Using Gaseous Methane and Liquid Oxygen," AIAA Paper 2006-4526, July 2006.

[3] Liao, S. M., and Zhao, T. S., "An Experimental Investigation of Convection Heat Transfer to Supercritical Carbon Dioxide in Miniature Tubes," *International Journal of Heat and Mass Transfer*, Vol. 45, 2002, pp. 5025–5034. doi:10.1016/S0017-9310(02)00206-5

[4] Pitla, S. S., Groll, E. A., and Ramadhyani, S., "New Correlation to Predict the Heat Transfer Coefficient During In-Tube Cooling of Turbulent Supercritical CO_2," *International Journal of Refrigeration*, Vol. 25, 2002, pp. 887–895. doi:10.1016/S0140-7007(01)00098-6

[5] Dang, C., and Hihara, E., "In-tube Cooling Heat Transfer of Supercritical Carbon Dioxide. Part 1. Experimental Measurement," *International Journal of Refrigeration*, Vol. 27, 2004, pp. 736–747. doi:10.1016/j.ijrefrig.2004.04.018

[6] Yun, R., Hwang, Y., and Radermacher, R., "Convective Gas Cooling Heat Transfer and Pressure Drop Characteristics of Supercritical CO_2/Oil Mixture in a Minichannel Tube," *International Journal of Heat and Mass Transfer*, Vol. 50, 2007, pp. 4796–4804. doi:10.1016/j.ijheatmasstransfer.2007.03.018

[7] Licht, J., Anderson, M., and Corradini, M., "Heat Transfer to Water at Supercritical Pressures in a Circular and Square Annular Flow Geometry," *International Journal of Heat and Fluid Flow*, Vol. 29, 2008, pp. 156–166. doi:10.1016/j.ijheatfluidflow.2007.09.007

[8] Koshizuka, S., Takano, N., and Oka, Y., "Numerical Analysis of Deterioration Phenomena in Heat Transfer to Supercritical Water," *International Journal of Heat and Mass Transfer*, Vol. 38, No. 16, 1995, pp. 3077–3084. doi:10.1016/0017-9310(95)00008-W

[9] Lee, S. H., and Howell, J. R., "Laminar Forced Convection at Zero Gravity to Water Near the Critical Region," *Journal of Thermophysics and Heat Transfer*, Vol. 10, No. 3, 1996, pp. 504–510. doi:10.2514/3.817

[10] Dang, C., and Hihara, E., "In-tube Cooling Heat Transfer of Supercritical Carbon Dioxide. Part 2. Comparison of Numerical Calculation with Different Turbulence Models," *International Journal of Refrigeration*, Vol. 27, 2004, pp. 748–760. doi:10.1016/j.ijrefrig.2004.04.017

[11] He, S., Jiang, P. X., Xu, Y. J., Shi, R. F., Kim, W. S., and Jackson, J. D., "A Computational Study of Convection Heat Transfer to CO_2 at Supercritical Pressures in a Vertical Mini Tube," *International Journal of Thermal Sciences*, Vol. 44, 2005, pp. 521–530. doi:10.1016/j.ijthermalsci.2004.11.003

[12] Zhang, X. R., and Yamaguchi, H., "Forced Convection Heat Transfer of Supercritical CO_2 in a Horizontal Circular Tube," *Journal of Supercritical Fluids*, Vol. 41, 2007, pp. 412–420. doi:10.1016/j.supflu.2006.11.003

[13] Pioro, I. L., Khartabi, H. F., and Duffey, R. B., "Heat Transfer to Supercritical Fluids Flowing in Channels—Empirical Correlations (Survey)," *Nuclear Engineering and Design*, Vol. 230, 2004, pp. 69–91. doi:10.1016/j.nucengdes.2003.10.010

[14] Duffey, R. B., and Pioro, I. L., "Experimental Heat Transfer of Supercritical Carbon Dioxide Flowing Inside Channels (Survey)," *Nuclear Engineering and Design*, Vol. 235, 2005, pp. 913–924. doi:10.1016/j.nucengdes.2004.11.011

[15] Hitch, B., and Karpuk, M., "Experimental Investigation of Heat Transfer and Flow Instabilities in Supercritical Fuels," AIAA Paper 1997-3043, July 1997.

[16] Chen, A. Y., and Dang, L., "Characterization of Supercritical JP-7's Heat Transfer and Coking Properties," AIAA Paper 2002-0005, Jan. 2002.

[17] Zhong, F., Fan, X., Yu, G., Li, J., Lu, X., and Sung, C. J., "Heat Transfer of Aviation Kerosene at Supercritical Conditions," *Journal of Thermophysics and Heat Transfer*, Vol. 23, No. 3, 2009, pp. 543–550. doi:10.2514/1.41619

[18] Pizzarelli, M., Nasuti, F., and Onofri, M., "Flow Analysis of Transcritical Methane in Rectangular Cooling Channels," AIAA Paper 2008-4556, July 2008.

[19] Mentor, F. R., "Two-Equation Eddy-Viscosity Turbulence Models for Engineering Applications," *AIAA Journal*, Vol. 32, No. 8, 1994, pp. 1598–1605. doi:10.2514/3.12149

[20] Cox, D. C., *Turbulence Modeling for CFD*, DCW Industries, La Cañada, CA, 1998.

[21] Meng, H., and Yang, V., "A Unified Treatment of General Fluid Thermodynamics and Its Application to a Preconditioning Scheme," *Journal of Computational Physics*, Vol. 189, 2003, pp. 277–304. doi:10.1016/S0021-9991(03)00211-0

[22] Meng, H., Hsiao, G. C., Yang, V., and Shuen, J. S., "Transport and Dynamics of Liquid Oxygen Droplets in Supercritical Hydrogen Streams," *Journal of Fluid Mechanics*, Vol. 527, 2005, pp. 115–139. doi:10.1017/S0022112004003106

[23] Ely, J. F., and Hanley, H. J. M., "Prediction of Transport Properties. 1. Viscosity of Fluids and Mixtures," *Industrial and Engineering Chemistry Fundamentals*, Vol. 20, No. 4, 1981, pp. 323–332. doi:10.1021/i100004a004

[24] Ely, J. F., and Hanley, H. J. M., "Prediction of Transport Properties. 2. Thermal Conductivity of Pure Fluids and Mixtures," *Industrial and Engineering Chemistry Fundamentals*, Vol. 22, No. 1, 1983, pp. 90–97. doi:10.1021/i100009a016

[25] Incropera, F. P., DeWitt, D. P., Bergman, T. L., and Lavine, A. S., *Fundamentals of Heat and Mass Transfer*, 6th ed., Wiley, New York, 2007.

[26] Jackson, J. D., and Hall, W. B., "Forced Convective Heat Transfer to Fluids at Supercritical Pressure," *Turbulence Forced Convection in Channels and Bundles*, edited by Kakac, S., and Spalding, D. B., Hemisphere, New York, 1979, pp. 563–612.

[27] Hua, Y.-X., Wang, Y. Z., and Meng, H., "A Numerical Study of Supercritical Forced Convective Heat Transfer of *n*-Heptane Inside a Horizontal Miniature Tube," *Journal of Supercritical Fluids*, Vol. 52, No. 1, 2010, pp. 36–46. doi:10.1016/j.supflu.2009.12.003